Sensors and Materials, Vol. 31, No. 4 (2019) 1273–1280
MYU Tokyo

S & M 1854

Photoluminescence and Scintillation Properties of Ce-doped $SrHfO_3$

Hiroyuki Fukushima,* Daisuke Nakauchi, Noriaki Kawaguchi, and Takayuki Yanagida

Division of Materials Science, Nara Institute of Science and Technology,
8916-5 Ikoma, Nara 630-0192, Japan

(Received November 29, 2018; accepted March 25, 2019)

Keywords: photoluminescence, scintillation, crystal, X-ray, $SrHfO_3$

Ce-doped $SrHfO_3$ crystals were synthesized by the floating zone (FZ) method, and their photoluminescence (PL) and scintillation properties were investigated. X-ray diffraction (XRD) measurement indicates that the samples are mainly composed of $SrHfO_3$, but a small peak due to HfO_2 is observed. In both PL and scintillation analyses, the Ce-doped samples show the emission peaking around 410 nm, whose decay time is short due to the 5d–4f transitions of Ce^{3+}. In the undoped sample, the emission appears around 480 nm. In the afterglow curves after 2 ms X-ray irradiation, no significant concentration dependence is observed.

1. Introduction

Scintillators emit numerous photons when interacting with ionizing radiations such as γ- and X-rays, and the applications of scintillators include positron emission tomography (PET) and X-ray computed tomography,[1,2] security,[3] nuclear plant,[4] environmental monitoring,[5] and well logging.[6] In general, high scintillation light yield, short decay time, low afterglow level, and high energy resolution are required as scintillation properties. Recently, some practical scintillators, such as rare-earth aluminum garnets,[7–9] and rare-earth silicates[10,11] contain Ce ions as a luminescent center and exhibit strong scintillation signals in UV-visible regions with a decay time range of 40−90 ns. For this reason, the Ce ion is an attractive activator for scintillators.[12–14]

In addition to the requirements mentioned above, γ- and X-ray detections require a high density and a high effective atomic number (Z_{eff}) to absorb energies and increase the detection efficiencies of high-energy photons.[15] Hafnium oxide materials such as $M$$HfO_3$ (M = Ca, Sr, or Ba) are promising candidates for novel γ- and X-ray scintillators because of their high density.[16,17] However, owing to the difficulties in crystal growth due to a high melting point (2730 °C),[18] the luminescence properties of $M$$HfO_3$ have been studied only in its powder or ceramic form.[19,20] Single crystal materials have a higher transparency than a powder or ceramic one, and in such a case, scintillation light can be effectively transported to photodetectors even in large scintillation detectors. In opaque materials such as powders or ceramics, the loss of

*Corresponding author: e-mail: fukushima.hiroyuki.ex8@ms.naist.jp
https://doi.org/10.18494/SAM.2019.2187

ISSN 0914-4935
https://myukk.org/

scintillation photons due to scattering and re-absorption becomes a problem, and principally, a large detector that enables us to achieve a high detection efficiency is impossible. Moreover, ideal crystal samples do not have grain boundaries, and it works sometimes to achieve a high conversion efficiency from the absorbed energy of ionizing radiation to scintillation photons. Although most commercial scintillators were synthesized by the Czochralski and Bridgman methods, which are suitable for the growth of single crystals in a large scale, it is difficult to prepare single crystals with high melting point by such melt growth techniques using a crucible. In recent years, the floating zone (FZ) method has been utilized for the material screening of single-crystal scintillators[21–23] and is suitable for preparing single crystals with a high melting point. Moreover, the synthesized crystals are protected from contaminations because FZ growth is performed without a crucible.[24] Recently, we have successfully synthesized some hafnium oxide compounds with high melting point by using a xenon arc lamp optical FZ.[25,26]

In our previous work, we have reported on the growth of a Ce-doped $CaHfO_3$ crystal, which has high Z_{eff} (65.15) and density (6.95 g/cm^3). The Ce-doped $CaHfO_3$ shows a high scintillation light yield of ~8100 photons/MeV,[26] which is comparable to that of a commercial $Bi_4Ge_3O_{12}$ scintillator (~8200 photons/MeV).[27] To achieve a higher detection efficiency against γ- and X-rays, we focused on $SrHfO_3$ with comparable Z_{eff} (63.10), but with a higher density (7.60 g/cm^3) than $CaHfO_3$. In this study, undoped and Ce-doped $SrHfO_3$ crystals were synthesized by the FZ method using a xenon arc lamp, and their photoluminescence (PL) and scintillation properties were evaluated.

2. Materials and Methods

$SrHfO_3$ crystals were synthesized using the FZ furnace with a xenon lamp (Crystal Systems Corporation, FZ-T-12000-X-VPO-PC-YH).[25] The concentrations of Ce were 0, 0.1, 1.0, and 3.0 at.% with respect to Sr. HfO_2 (99.95%, Furuuchi Chemical), $SrCO_3$ (99.99%, Wako Pure Chemical), and CeO_2 (99.99%, Furuuchi Chemical) powders were used as raw materials. The mixture was calcined at 1100 ℃ for 8 h to release carbonate. The sintered powder was formed into a cylinder loaded in a balloon. Moreover, the cylindrical rod was sintered at 1500 ℃ for 8 h in air. The crystal growth in the FZ furnace was conducted at a pull-down rate of 30 mm/h and a rotation rate of 3 rpm. The powder X-ray diffraction (XRD) patterns were investigated using a diffractometer (Rigaku, MiniFlex600) using a CuKα micro X-ray tube (40 kV and 15 mA) in the range of $2\theta = 10–80°$.

The PL excitation (PLE) and PL contour plots, and PL quantum yield (QY) were evaluated using a Quantaurus-QY spectrometer (Hamamatsu Photonics, C11347). The PL decay curve under excitation at 280 nm was measured using a Quantaurus-τ spectrometer (Hamamatsu Photonics, C11367). Here, the monitoring wavelengths of undoped and Ce-doped samples were 400 and 410 nm, respectively. Moreover, to determine the origin of afterglow seen by the naked eye, the undoped and 0.3% Ce-doped samples were measured at 480 nm.

To obtain X-ray-induced scintillation spectra, an X-ray generator (Spellman, XRB80N100/CB) was equipped with an X-ray tube supplied with 80 kV and 1.2 mA. The equipment was reported in detail previously.[7] The scintillation emission was guided to the spectrometer

(Andor, DU-430-BU2 CCD with a Shamrock SR163 monochromator) using a 2 m optical fiber to measure a spectrum. The X-ray-induced scintillation decay time curves and afterglow characterization were evaluated using an afterglow characterization system.[28]

3. Results and Discussion

Figure 1(a) shows a photograph of the synthesized undoped and Ce-doped $SrHfO_3$ crystals. The undoped sample appears colorless, while the Ce-doped samples appear yellow. The sizes of the as-prepared crystals are 10−20 mm. The cylindrical samples were cut along the growth direction to evaluate their PL and scintillation properties. The cut samples have a diameter of 4−5 mm and a length of 1−2 mm. Figure 1(b) indicates photographs of the 0.3% Ce-doped sample during and after UV (302 nm) irradiation. The 0.3% Ce-doped sample shows a cyan emission at the edge of the sample during UV irradiation, and a long afterglow was clearly observed by the naked eye after UV irradiation. As described later, the green emission at the rim of the samples would be blamed for the emission of the remaining HfO_2, and this means that the stoichiometric composition would not be adequate for $SrHfO_3$ in the melt growth. To obtain more uniform and transparent samples, the preparation of samples with nonstoichiometric composition may be helpful.

Figure 2 shows the powder XRD patterns of the samples. The peak positions are roughly in agreement with the reference $SrHfO_3$ (COD 1010425), which belongs to the *Pnma* space group of the orthorhombic crystal system.[29] However, the XRD patterns show a weak peak around 28°, which is not observed in the reference pattern. Monoclinic HfO_2 has numerous diffraction peaks, and one of the peaks was considered to correspond to the peak around 28°. Hence, the long afterglow shown in Fig. 1(b) is attributed to HfO_2.[30]

Figure 3 shows the PLE-PL contour plots of the undoped and Ce-doped $SrHfO_3$ crystals. Under excitation around 310 nm, an emission band appears around 480 nm in the undoped sample, while the Ce-doped samples show PL peaking around 410 nm; these results are almost

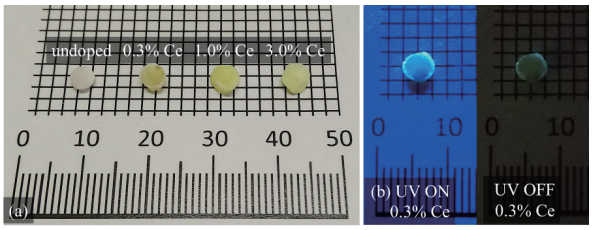

Fig. 1. (Color online) Photograph of (a) synthesized undoped and Ce-doped $SrHfO_3$ crystals, and (b) comparison of the 0.3% Ce-doped sample characteristics observed during and after UV (302 nm) irradiation.

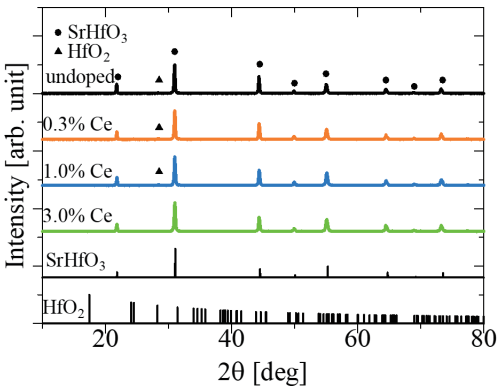

Fig. 2. (Color online) Powder XRD patterns of undoped and Ce-doped $SrHfO_3$ crystals as well as the references orthorhombic $SrHfO_3$ and monoclinic HfO_2.

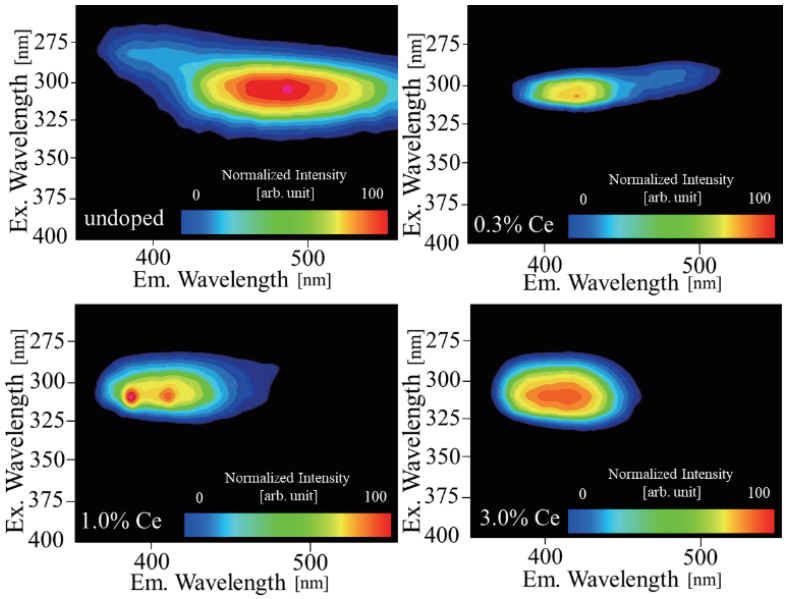

Fig. 3. (Color online) PLE-PL contour plots of undoped and Ce-doped $SrHfO_3$ crystals. Em. and Ex. mean emission and excitation, respectively.

the same as those previously reported in ceramic samples.[31] The PL QYs of the undoped and 0.1, 1.0, and 3.0% Ce-doped samples are 15.9, 9.8, 6.5, and 6.6%, respectively. The emission origin of the Ce-doped samples would be the 5d–4f transitions of Ce^{3+}, and the emission around 480 nm observed in the undoped sample is considered to be HfO_2.[32] The 0.3% Ce-doped sample also shows a weak emission around 480 nm, and the PL decay curves of the undoped and 0.3% Ce-doped samples exhibit a long component described later.

Figure 4 shows PL decay curves of the undoped and Ce-doped $SrHfO_3$ crystals under excitation at 280 nm monitored at 400 and 410 nm, respectively. In addition, the undoped and 0.3% Ce-doped sample were measured under excitation at 280 nm monitored at 480 nm. Table 1 shows the decay times determined from the decay curves. The undoped and 0.3% Ce-doped samples were approximated by a sum of three exponential decay components, and the decay curves of the 1.0 and 3.0% Ce-doped samples have two components. The first decay component is due to an instrumental response function in all the data, and the second decay component (τ_1) of the Ce-doped samples indicates a longer decay time than powder Ce-doped $SrHfO_3$,[19] which may have been caused by the difference in dopant concentration. The second decay component (τ_1) of the undoped sample would be due to some defects. The third component (τ_2) of the undoped and 0.3% Ce-doped samples is considered to be due to monoclinic HfO_2. To consider the origin of the emission around 480 nm observed in Fig. 3, the PL decay curves were measured by monitoring at 480 nm as shown in the inset of Fig. 4. The decay constants of the undoped (6.5 μs) and 0.3% Ce-doped (7.1 μs) samples are close to that of the monoclinic HfO_2,[30] and the emission wavelength is also similar to that of HfO_2. Hence, the undoped and 0.3% Ce-doped samples are considered to contain a small amount of HfO_2.

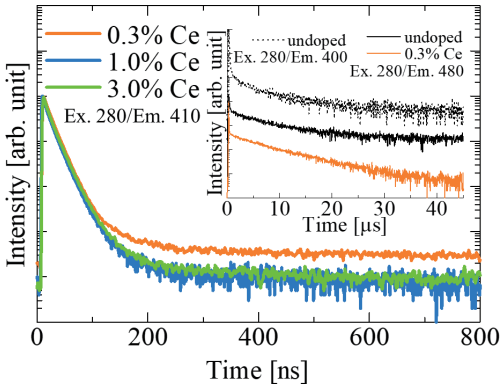

Fig. 4. (Color online) PL decay curves of Ce-doped samples monitored at 410 nm. The inset shows PL decay curves of undoped and 0.3% Ce-doped samples monitored at 400 (dashed line) and 480 (solid line) nm, respectively.

Table 1
PL decay times of undoped and Ce-doped $SrHfO_3$ samples monitored at 400 and 410 nm, respectively.

	τ_1	τ_2
undoped	86.6 ns	4.6 μs
0.3% Ce	46.9 ns	581.5 ns
1.0% Ce	48.7 ns	—
3.0% Ce	51.1 ns	—

Figure 5 shows X-ray-induced scintillation spectra of the undoped and Ce-doped samples. The emission of all the samples appears around 410 nm. The undoped sample was measured using the transmission geometry, while the Ce-doped samples were evaluated using the reflection geometry to prevent self-absorption caused by the 4f–5d transitions of Ce^{3+}. The spectra of all the samples were similar to that of a powder sample, which has a spectral range of 350−500 nm.[19] In the powder sample, the emission in the UV range was highly self-absorbed,[19] and a clear observation of UV emission was a merit of using crystalline samples. However, the undoped sample as well as the 0.3 and 1.0 % Ce-doped samples have a spectral range up to 650 nm. Moreover, the X-ray-induced scintillation spectra show a similar emission tendency to the PLE-PL contour plots as shown in Fig. 3. Thus, the longer wavelength emission is considered to due to a residual of HfO_2.[30] When we attempted to measure a pulse height spectrum, the photoabsorption peak was unclear owing to the low light yield and energy resolution due to the nonuniformity of the samples. The use of samples prepared nonstoichiometrically would help to improve crystallinity and transparency because some results suggest an excess of HfO_2.

Figure 6 shows X-ray-induced scintillation decay curves of the undoped and Ce-doped samples. Table 2 shows the components of the X-ray-induced scintillation decay curves. The decay curve of the undoped sample was approximated by a sum of three exponential components. Here, the first component is due to an instrumental response function in this time range, and the decay time constants of the second component (τ_1) and third component (τ_2) are close to those in PL. Hence, the emission origin of the second and third components would be some defects in the host and HfO_2, respectively. The decay curves of Ce-doped samples were approximated by a sum of two exponential decay components. The second component (τ_1) would be due to the 5d–4f transitions of Ce^{3+}.

Figure 7 shows the afterglow curves obtained after 2 ms X-ray irradiation. The afterglow level (A) is defined as $A = 100 \times (I_2 - I_0)/(I_1 - I_0)$, where I_0, I_1, and I_2 denote the mean signal

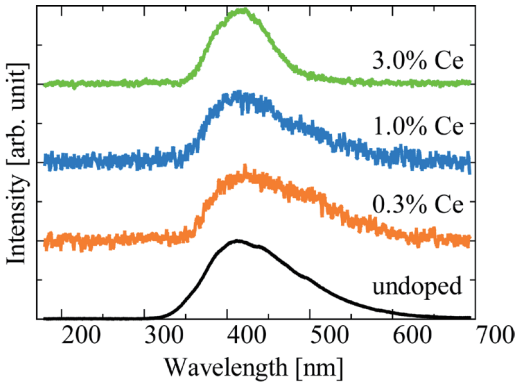

Fig. 5. (Color online) X-ray-induced scintillation spectra of undoped and Ce-doped $SrHfO_3$ samples. The undoped sample was measured using the transmittance geometry, and the Ce-doped samples were evaluated using the reflection geometry.

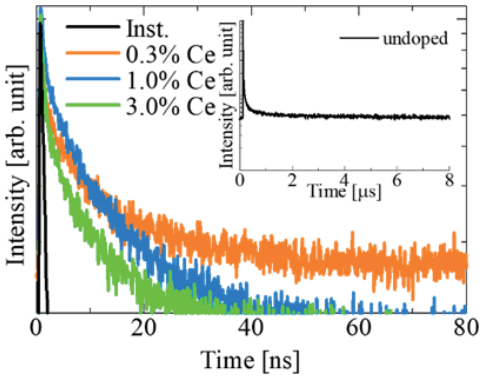

Fig. 6. (Color online) X-ray-induced scintillation decay curves of undoped (inset) and Ce-doped $SrHfO_3$ samples, and the signals of an instrumental response function (Inst.) are also drawn.

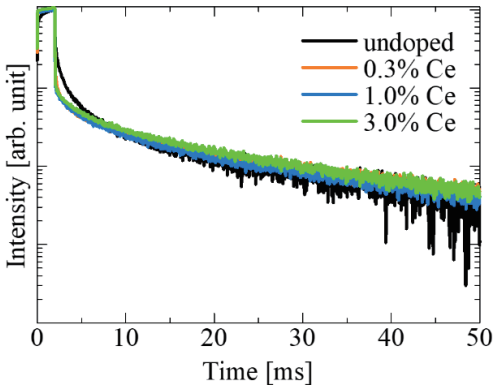

Fig. 7. (Color online) Afterglow curves of undoped and Ce-doped $SrHfO_3$ samples after 2 ms X-ray irradiation.

Table 2
X-ray-induced scintillation decay constants and afterglow levels of undoped and Ce-doped $SrHfO_3$ samples.

	τ_1 (ns)	τ_2 (μs)	Afterglow level (ppm)
undoped	86.5	4.6	1.0×10^4
0.3% Ce	13.3	—	1.3×10^4
1.0% Ce	12.6	—	1.1×10^4
3.0% Ce	16.2	—	1.3×10^4

intensity before the X-ray irradiation, the mean signal intensity during the irradiation, and the signal intensity at t = 20 ms after the irradiation, respectively. Table 2 shows the calculated afterglow levels of the samples, which were quite higher than those of the practical scintillators.[28] The afterglow of HfO_2 is extremely long,[30] and the samples may contain a small amount of HfO_2 as mentioned above. Hence, the high afterglow levels were considered to be due to the residual of HfO_2 in the samples.

4. Conclusions

Undoped and Ce-doped $SrHfO_3$ crystals were synthesized by the FZ method using a xenon arc lamp. Suggested from the XRD patterns, the crystal samples seem to have the impurity of HfO_2. The undoped sample shows PL and scintillation around 480 and 410 nm, respectively. The Ce-doped samples show a broad emission band around 410 nm and a short decay time

due to the 5d–4f transitions of Ce^{3+} in both PL and X-ray-induced scintillation. The emission wavelength of all the samples is suitable for PMT sensitivity. The afterglow levels are almost the same among the samples. To improve scintillation light yield and afterglow properties, the impurity HfO_2 phase should be removed.

Acknowledgments

This work was supported by Grants-in-Aid for Scientific Research A (17H01375), Scientific Research B (18H03468), and JSPS Research Fellow (17J09488) from JSPS. The Cooperative Research Project of Research Institute of Electronics, Shizuoka University, Terumo Foundation for Life Sciences and Arts, Izumi Science and Technology Foundation, The Kazuchika Okura Memorial Foundation, The Iwatani Naoji Foundation, and NAIST Foundation are also acknowledged.

References

1 T. K. Lewellen: Phys. Med. Biol. **53** (2008) R287.
2 M. E. Phelps, E. J. Hoffman, N. A. Mullani, and M. M. Ter-Pogossian: J. Nucl. Med. **16** (1975) 210.
3 G. Harding: Radiat. Phys. Chem. **71** (2004) 869.
4 Y. Shirakawa: Nucl. Instrum. Methods Phys. Res., Sect. B **263** (2007) 58.
5 K. Watanabe, T. Yanagida, K. Fukuda, A. Koike, T. Aoki, and A. Uritani: Sens. Mater. **27** (2015) 1.
6 T. Yanagida, Y. Fujimoto, S. Kurosawa, K. Kamada, H. Takahashi, Y. Fukazawa, M. Nikl, and V. Chani: Jpn. J. Appl. Phys. **52** (2013) 076401.
7 T. Yanagida, K. Kamada, Y. Fujimoto, H. Yagi, and T. Yanagitani: Opt. Mater. **35** (2013) 2480.
8 T. Yanagida, H. Takahashi, T. Ito, D. Kasama, T. Enoto, M. Sato, S. Hirakuri, M. Kokubun, K. Makishima, T. Yanagitani, H. Yagi, T. Shigeta, and T. Ito: IEEE Trans. Nucl. Sci. **52** (2005) 1836.
9 T. Oya, D. Nakauchi, G. Okada, N. Kawaguchi, and T. Yanagida: Nucl. Instrum. Methods Phys. Res., Sect. A **866** (2017) 134.
10 A. Nassalski, M. Kapusta, T. Batsch, D. Wolski, D. Mockel, W. Enghardt, and M. Moszynski: IEEE Nucl. Sci. Symp. Conf. Rec. 2005 (IEEE, 2005) 2823–2829.
11 L. Pidol, A. Kahn-Harari, B. Viana, E. Virey, B. Ferrand, P. Dorenbos, J. T. M. de Haas, and C. W. E. van Eijk: IEEE Trans. Nucl. Sci. **51** (2004) 1084.
12 H. Kimura, F. Nakamura, T. Kato, D. Nakauchi, G. Okada, N. Kawaguchi, and T. Yanagida: Sens. Mater. **30** (2018) 1555.
13 Y. Fujimoto, K. Saeki, D. Nakauchi, T. Yanagida, M. Koshimizu, and K. Asai: Sens. Mater. **29** (2017) 1425.
14 G. Okada, M. Akatsuka, H. Kimura, M. Mori, N. Kawano, N. Kawaguchi, and T. Yanagida: Sens. Mater. **30** (2018) 1547.
15 Y. Fujimoto, K. Saeki, D. Nakauchi, T. Yanagida, M. Koshimizu, and K. Asai: Sens. Mater. **30** (2018) 1577.
16 W. Jia, D. Jia, T. Rodriguez, Y. Wang, H. Jiang, and K. Li: J. Lumin. **122**–**123** (2007) 55.
17 I. E. Seferis, K. Fiaczyk, D. Spassky, E. Feldbach, I. Romet, M. Kirm, and E. Zych: J. Lumin. **189** (2017) 148.
18 H. Rétot, A. Bessière, A. Kahn-Harari, and B. Viana: Opt. Mater. **30** (2008) 1109.
19 M. Nikl, P. Bohacek, B. Trunda, V. Jary, P. Fabeni, V. Studnicka, R. Kucerkova, and A. Beitlerova: Opt. Mater. **34** (2011) 433.
20 E. V. van Loef, W. M. Higgins, J. Glodo, C. Brecher, A. Lempicki, V. Venkataramani, W. W. Moses, S. E. Derenzo, and K. S. Shah: IEEE Trans. Nucl. Sci. **54** (2007) 741.
21 D. Nakauchi, G. Okada, N. Kawano, N. Kawaguchi, and T. Yanagida: Appl. Phys. Express **10** (2017) 072601.
22 M. Akatsuka, Y. Usui, D. Nakauchi, G. Okada, N. Kawaguchi, and T. Yanagida: Sens. Mater. **30** (2018) 1525.
23 N. Kumamoto, D. Nakauchi, T. Kato, G. Okada, N. Kawaguchi, and T. Yanagida: Sens. Mater. **29** (2017) 1417.
24 S. Kimura and I. Shindo: J. Cryst. Growth **41** (1977) 192.
25 D. Nakauchi, G. Okada, N. Kawaguchi, and T. Yanagida: Jpn. J. Appl. Phys. **57** (2018) 100307.
26 H. Fukushima, D. Nakauchi, G. Okada, N. Kawaguchi, and T. Yanagida: J. Mater. Sci. Mater. Electron. **29** (2018) 21033.

27 I. Holl, E. Lorenz, and G. Mageras: IEEE Trans. Nucl. Sci. **35** (1988) 105.
28 T. Yanagida, Y. Fujimoto, T. Ito, K. Uchiyama, and K. Mori: Appl. Phys. Express **7** (2014) 062401.
29 A. Feteira, D. C. Sinclair, K. Z. Rajab, and M. T. Lanagan: J. Am. Ceram. Soc. **91** (2008) 893.
30 A. Wiatrowska, E. Zych, and L. Kępiński: Radiat. Meas. **45** (2010) 493.
31 Y. M. Ji, D. Y. Jiang, Z. H. Wu, T. Feng, and J. L. Shi: Mater. Res. Bull. **40** (2005) 1521.
32 K. Fiaczyk, A. J. Wojtowicz, and E. Zych: J. Phys. Chem. C **119** (2015) 5026.